JOURNAL OF EXPERIMENTAL AND THEORETICAL PHYSICS, 2024, Vol. 166, No. 6 (12), pp. 803–814

ORDER, DISORDER, AND PHASE TRANSITION IN CONDENSED MEDIA

THE ROLE OF MAGNETOELASTIC INTERACTIONS IN FeRh ALLOY AT ANTIFERRO-FERROMAGNETIC PHASE TRANSITION

© 2024 I. S. Kozvonin[a], A. A. Tereshchenko[a], A. S. Ovchinnikov[a]*, N. V. Baranov[b], E. Z. Valiev[b]

[a] Institute of Natural Sciences and Mathematics, Ural Federal University, Yekaterinburg, 620083 Russia

[b] Institute of Metal Physics, Ural Branch of the Russian Academy of Sciences, Yekaterinburg, 620219 Russia

*e-mail: alexander.ovchinnikov@urfu.ru

Received June 05, 2024

Revised August 16, 2024

Accepted August 20, 2024

Abstract. To explain the features of magnetic phase transitions in FeRh alloy, an effective mean-field theory is proposed that takes into account the interaction of elastic and magnetic degrees of freedom. Along with the magnetization of iron atom sublattices and mean values of the uniform compression deformation and uniaxial tension strains, the order parameter of the theory also includes internal magnetic field causing the appearance of non-zero magnetization of rhodium atoms during the antiferro-ferromagnetic phase transition. Within this theory, it is possible to calculate the temperature dependencies of total magnetization and relative volume change that agree with experimental data, and to show that the antiferro-ferromagnetic transition is a first-order phase transition. The choice of exchange interaction constants, consistent with *ab initio* calculations of electronic structure, reveals the leading mechanism of this transition — the renormalization of exchange interaction between nearest neighbors in the iron atom subsystem, arising when considering two-ion magnetoelastic interaction. It is shown that thermal excitation of spin waves contributes to the enhancement of uniaxial strains, reducing the cubic symmetry of the lattice to tetragonal.

DOI: 10.31857/S004445102412e06X

1. INTRODUCTION

Explaining the magnetic properties of the FeRh alloy remains a challenging task for many decades, despite the seemingly simple nature of magnetic transitions observed in this compound. Thus, in the ordered FeRh alloy, with increasing temperature, a first-order phase transition from antiferromagnetic (AFM) phase to ferromagnetic (FM) phase is observed [1,2]. This transition occurs at temperature T_0, varying in the range from room temperature to approximately 400 K. The transition temperature strongly depends on the composition and presence of crystal structure defects [3]. The phase transition is accompanied by a volume increase of approximately 1%, while the body-centered crystal structure of CsCl-type remains unchanged [4, 5]. However, some theoretical calculations show that orthorhombic or tetragonal distortions in the AFM phase contribute to its stabilization [6]. Regarding magnetization behavior, early neutron diffraction experiments established that in the AFM phase, only iron atoms have a magnetic moment $\mu_{Fe} \approx 3.2\mu_B$ ($\mu_{Rh} = 0$), while at temperatures above T_0 a magnetic moment appears on rhodium atoms $\mu_{Rh} \sim 1\mu_B$, but μ_{Fe} changes only slightly [7, 8]. Additionally, during the AFM–FM transition, anomalously large changes in magnetic entropy [9, 10], electrical resistance [11], and forced volume magnetostriction [12] are observed. A detailed description of the main studies of magnetic and magnetocaloric properties of FeRh alloys is contained in review [13]. All these facts together make FeRh a promising material for use in next-generation memory devices, magnetic cooling systems, and magnetostriction devices, despite the low abundance and high cost of rhodium.

To explain the nature of the AFM–FM transition, several mechanisms were proposed, in particular, the Kittel model with inversion of exchange interaction sign between iron atoms [14] and the exchange-striction model of ferromagnets [15, 16]. Currently,

there are several theoretical works containing results of *ab initio* calculations of the compound's electronic structure FeRh [17, 18]. However, it must be acknowledged that there is still no consensus on the cause of this phase transition.

One of the open problems in the theory of AFM–FM transition is explaining the absence of magnetic moment on rhodium atoms at low temperatures. *Ab initio* calculations give a sufficiently large value for ferromagnetic Fe–Rh exchange [19], which should lead to stabilization of the FM phase at low temperatures. To explain this anomaly, in work [20], it was suggested that the immersion of 4*d* Rh electron zone, slightly split by exchange interaction, below the Fermi level to a depth ensuring its complete filling at temperature $T = 0$ K, explains the spin compensation of 4*d* electrons in the low-temperature AFM phase. The emergence of non-zero magnetic moment was attributed by the authors to thermal blurring of the Fermi level and the appearance of holes in the 4*d* zone *in the absence of atomic structure distortions*. The latter assumption was supported by experimental data from femtosecond optics [21, 22], indicating that changes in spin structure precede changes in atomic structure.

In our view, regardless of what triggers the appearance of non-zero magnetization in the rhodium atoms subsystem, such exclusion of structural transitions from consideration does not allow for a consistent description of the AFM–FM transition. The data accumulated to date on the study of magnetically ordered BCC alloys with substitution Fe(RhM), where M=Fe, Co, Ni, Pd, Ir, Pt [23], Fe(RhPd) [24], FeRhCr (with chromium substitutions of both iron and rhodium) [25] and (Fe,Ru)Rh [26] convincingly demonstrate a close correlation between the AFM–FM transition temperature, the magnitude of μ_{Ru} and the parameters of the crystal atomic lattice.

The aim of this work is to construct a mean-field theory that effectively accounts for the restructuring of the spin-polarized state density of Rh atoms at the AFM–FM transition point, linking it *with changes in elastic deformations*. In this regard, our consideration represents a generalization and development of ideas from previous studies using magnetoelastic interactions to describe the specifics of the AFM–FM transition in FeRh alloy [14–16]. Also, within our approach, we take into account the results of *ab initio* electronic structure calculations for FeRh presented in [19], according to which it is necessary to consider the exchange interaction between iron atoms up to the nearest neighbors from the third coordination sphere. Elastic and magnetoelastic interactions are described in our model based on the cubic symmetry of the FeRh crystal, which allows determining structural order parameters associated with the uniform compression deformation strain and uniaxial strain that reduces cubic symmetry to tetragonal. The main feature of considering magnetic degrees of freedom lies in the fact that the temperature behavior of rhodium atoms' magnetization is considered a known predetermined function, and within the self-consistent procedure, the conjugate internal field and magnetizations of two iron atom sublattices are calculated. Such formulation corresponds to the statistical model of a grand canonical ensemble, where the role of the observable average number of particles is played by the magnetization of the rhodium atom subsystem, and the role of chemical potential is played by the conjugate internal magnetic field. The growth of this field at point T_0 will effectively correspond to the restructuring of the spin-polarized electronic state density of Rh at the Fermi level, ensuring the appearance of non-zero μ_{Rh}.

Within this description, it is possible to show that the AFM–FM transition has the character of a first-order phase transition, where above the temperature T_0 along with the stable FM phase, remnants of the AFM phase will be observed. The presented theory allows obtaining temperature dependencies of total magnetization and relative volume change of FeRh throughout the entire temperature range, which are consistent with experimental data. It also reveals the leading mechanism of the AFM–FM transition associated with magnetoelastic interaction, accounting for which leads to temperature renormalization of effective exchange interaction between nearest iron atoms. As a result, the latter contributes to the stabilization of the AFM phase at low temperatures, and near T_0 it, sharply decreasing in magnitude and changing its sign, shifts the balance of exchange interactions in favor of FM order. Finally, our analysis explains the emergence of tetragonal deformations and, in particular, shows that thermal excitation of spin waves contributes to their growth.

The article is organized as follows. Section 2 presents a model of exchange, elastic, and magnetoelastic

interactions in FeRh alloy. Section 3 formulates the mean-field theory for describing magnetic and structural transitions of this compound. The choice of model parameters and features of theory equation solutions are discussed in Section 4. Section 5 analyzes changes in equilibrium deformations of the atomic lattice arising from spin-wave fluctuations using the technique of two-time Green's functions. Conclusions are contained in Section 6.

2. MODEL

To describe magnetoelastic interaction in FeRh, we use a model Hamiltonian

$$\mathcal{H} = \mathcal{H}_m + \mathcal{H}_{el} + \mathcal{H}_{me} + \mathcal{H}_T, \tag{1}$$

where the magnetic part

$$\mathcal{H}_m = -J_1 \sum_{\mathbf{n},\boldsymbol{\delta}_1} \mathbf{S}_\mathbf{n} \cdot \mathbf{S}_{\mathbf{n}+\boldsymbol{\delta}_1} - J_2 \sum_{\mathbf{n},\boldsymbol{\delta}_2} \mathbf{S}_\mathbf{n} \cdot \mathbf{S}_{\mathbf{n}+\boldsymbol{\delta}_2} - \\ -J_3 \sum_{\mathbf{n},\boldsymbol{\delta}_3} S_\mathbf{n} \cdot S_{\mathbf{n}+\boldsymbol{\delta}_3} - J \sum_{\mathbf{n},\boldsymbol{\delta}} s_\mathbf{n} \cdot S_{\mathbf{n}+\boldsymbol{\delta}} \tag{2}$$

describes the exchange magnetic interaction between magnetic moments of iron atoms ($\mathbf{S_n}$) in three coordination spheres of smallest radius (Fig. 1) and between magnetic moments of nearest neighbor Fe atoms and Rh ($\mathbf{s_n}$). Here δ_i is the position vector of iron atoms from the ith coordination sphere ($i = 1,2,3$), and J_i — the magnitude of exchange interaction between these atoms and the iron atom located in the central node, J is the exchange interaction constant Fe–Rh.

The Hamiltonian of elastic deformations in a crystal with cubic symmetry is defined by the expression [27]

$$\mathcal{H}_{el} = \frac{1}{2} c_{11}(u_{xx}^2 + u_{yy}^2 + u_{zz}^2) + \\ + c_{12}(u_{xx}u_{yy} + u_{xx}u_{zz} + u_{yy}u_{zz}) + \\ + 2c_{44}(u_{yz}^2 + u_{xz}^2 + u_{xy}^2), \tag{3}$$

where u_{ij} are components of the strain tensor, and c_{ij} are the corresponding elastic coefficients.

Magnetoelastic interaction is considered within the two-ion model, where its role is reduced to changing the exchange interaction due to elastic deformations. The corresponding contribution to the Hamiltonian for a pair of sites (**m, n**) has the form [28]

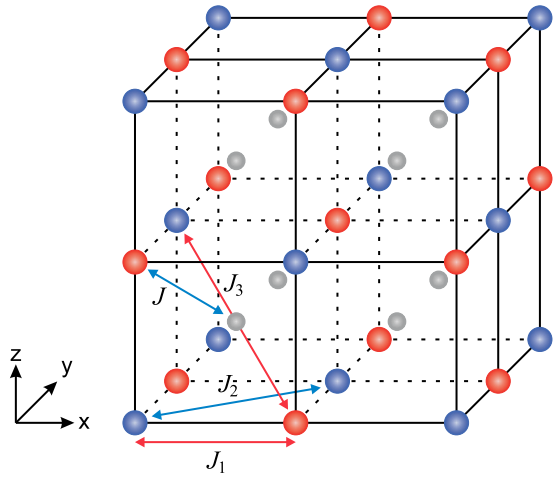

Fig. 1. Extended unit cell of FeRh. The colors indicate iron atoms of the first sublattice (red), second sublattice (blue), and rhodium atoms (gray)

$$\mathcal{H}_{me}(\mathbf{m},\mathbf{n}) = -D_1(u_{xx} + u_{yy} + u_{zz})(\mathbf{S_m} \cdot \mathbf{S_n}) - \\ -\frac{1}{4} D_2 \left[(u_{xx} - u_{yy}) \left(\mathbf{S}_\mathbf{m}^x \mathbf{S}_\mathbf{n}^x - \mathbf{S}_\mathbf{m}^y \mathbf{S}_\mathbf{n}^y \right) + \right. \\ \left. + \frac{1}{3} (2u_{zz} - u_{xx} - u_{yy}) \left(2\mathbf{S}_\mathbf{m}^z \mathbf{S}_\mathbf{n}^z - \mathbf{S}_\mathbf{m}^x \mathbf{S}_\mathbf{n}^x - \mathbf{S}_\mathbf{m}^y \mathbf{S}_\mathbf{n}^y \right) \right] - \\ -\frac{1}{2} D_3 [u_{xy} \left(\mathbf{S}_\mathbf{m}^x \mathbf{S}_\mathbf{n}^y + \mathbf{S}_\mathbf{m}^y \mathbf{S}_\mathbf{n}^x \right) + u_{yz} \left(\mathbf{S}_\mathbf{m}^y \mathbf{S}_\mathbf{n}^z + \mathbf{S}_\mathbf{m}^z \mathbf{S}_\mathbf{n}^y \right) + \\ + u_{xz} \left(\mathbf{S}_\mathbf{m}^x \mathbf{S}_\mathbf{n}^z + \mathbf{S}_\mathbf{m}^z \mathbf{S}_\mathbf{n}^x \right)], \tag{4}$$

where D_a ($a = 1,2,3$) are magnetoelastic interaction coefficients corresponding to certain basic combinations of spin operators allowed by cubic symmetry.

As shown by *ab initio* calculations of the FeRh electronic structure [19], the exchange interaction between nearest-neighbor iron atoms proves to be most sensitive to changes in interatomic distance. Therefore, in our model, we will consider magnetoelastic interactions only for such pairs of magnetic moments. The corresponding contribution to the total Hamiltonian (1) can be represented as

$$\mathcal{H}_{me} = \sum_{\mathbf{n},\boldsymbol{\delta}_1} \mathcal{H}_{me}(\mathbf{n}, \mathbf{n} + \boldsymbol{\delta}_1). \tag{5}$$

The term $\mathcal{H}_T$ accounts for crystal deformation associated with thermal expansion, which differs from deformation caused by magnetoelastic interaction. It can be chosen in the standard form [29]

$$\mathcal{H}_T = -\alpha(T - T_0)(u_{xx} + u_{yy} + u_{zz}). \tag{6}$$

It is assumed that thermal deformations are absent at the AFM–FM transition temperature T_0, where a jump in the relative volume change is observed [5]. The latter, within our model, is exclusively associated with the role of magnetoelastic interaction, while $\mathcal{H}_T$ explicitly depends on the thermal expansion coefficient α, determined by anharmonic contributions to the crystal potential energy as a function of atomic displacements [30]. As will be shown in our calculations, accounting for anharmonic effects is important at high temperatures.

3. MEAN FIELD THEORY

To describe the magnetic AFM–FM transition in FeRh, let us first consider the Hamiltonian (1) within the mean field approximation, where the order parameters are the magnetizations of two iron atom sublattices $\langle S^z_{1,2}\rangle$, the magnetization of the rhodium atom sublattice $\langle s^z\rangle$, as well as equilibrium deformations of uniform compression $\langle u_{xx}+u_{yy}+u_{zz}\rangle$ and uniaxial extension $\langle 2u_{zz}-u_{xx}-u_{yy}\rangle/3$.

For further calculations, it is convenient to choose an extended elementary cell containing 4 spins of two iron atom sublattices and 8 spins of rhodium atoms (Fig. 1).

Then the magnetic part of the Hamiltonian can be represented as

$$\mathcal{H}_m = NE_0^{(m)} - \sum_{i=1}^{4N} H_1^{(m)} S^z_{1i} - \sum_{i=1}^{4N} H_2^{(m)} S^z_{2i} - \sum_{i=1}^{8N} H_3^{(m)} s^z_i, \quad (7)$$

in which N is the number of extended elementary cells, and the ground state energy is determined by the expression

$$E_0^{(m)} = 24J_1\langle S_1^z\rangle\langle S_2^z\rangle + 24J_2\Big(\langle S_1^z\rangle^2 + \langle S_2^z\rangle^2\Big) + 32J_3\langle S_1^z\rangle\langle S_2^z\rangle + 32J\langle s^z\rangle\Big(\langle S_1^z\rangle + \langle S_2^z\rangle\Big).$$

The remaining terms in the Hamiltonian (7) describe the local interactions of spins of the first and second sublattices of atoms Fe, S^z_{1i} and S^z_{2i} respectively, as well as the spins of atoms Rh, s^z_i with molecular fields

$$H_1^{(m)} = z_1J_1\langle S_2^z\rangle + z_2J_2\langle S_1^z\rangle + z_3J_3\langle S_2^z\rangle + 2z_4J\langle s^z\rangle, \quad (8)$$

$$H_2^{(m)} = z_1J_1\langle S_1^z\rangle + z_2J_2\langle S_2^z\rangle + z_3J_3\langle S_1^z\rangle + 2z_4J\langle s^z\rangle, \quad (9)$$

$$H_3^{(m)} = z_4J\Big(\langle S_1^z\rangle + \langle S_2^z\rangle\Big). \quad (10)$$

Here

$$z_1 = 6, \qquad z_2 = 12, \qquad z_3 = 8, \qquad z_4 = 4$$

represent the numbers of nearest neighbors of the corresponding coordination spheres.

The magnetoelastic part of the Hamiltonian (1) in the mean field approximation takes the form

$$\mathcal{H}_{me} = NE_0^{(me)} - \sum_{i=1}^{4N} H_1^{(me)} S^z_{1i} - \sum_{i=1}^{4N} H_2^{(me)} S^z_{2i}, \quad (11)$$

where

$$E_0^{(me)} = [24D_1(u_{xx}+u_{yy}+u_{zz}) + 4D_2(2u_{zz}-u_{xx}-u_{yy})]\langle S_1^z\rangle\langle S_2^z\rangle.$$

Corrections to molecular fields contain contributions from all-round compression deformations and uniaxial tension

$$H_{1,2}^{(me)} = z_1D_1(u_{xx}+u_{yy}+u_{zz})\langle S^z_{2,1}\rangle + \frac{1}{6}z_1D_2(2u_{zz}-u_{xx}-u_{yy})\langle S^z_{2,1}\rangle. \quad (12)$$

Using the standard procedure, one can obtain an expression for the free energy of the lattice and magnetic subsystems per volume of the extended elementary cell $V_0 = 8a^3$ (a is the constant of the cubic lattice FeRh)

$$\mathcal{F} = \frac{1}{2}c_{11}V_0(u_{xx}^2+u_{yy}^2+u_{zz}^2) + c_{12}V_0(u_{xx}u_{yy}+u_{xx}u_{zz}+u_{yy}u_{zz}) + 2c_{44}V_0(u_{yz}^2+u_{xz}^2+u_{xy}^2) + E_0^{(m)} + E_0^{(me)} - \alpha(T-T_0)(u_{xx}+u_{yy}+u_{zz}) - \frac{4}{\beta}\sum_{\alpha=1,2}\ln\left\{\frac{\left[\beta\Big(S+1/2\Big)\Big(H_\alpha^{(m)}+H_\alpha^{(me)}\Big)\right]}{\left[\beta\Big(H_\alpha^{(m)}+H_\alpha^{(me)}\Big)/2\right]}\right\} - \frac{8}{\beta}\ln\left\{\frac{\left[\beta\Big(s+1/2\Big)H_3^{(m)}\right]}{\left[\beta H_3^{(m)}/2\right]}\right\}, \quad (13)$$

in which $\beta = 1/k_BT$, k_B is the Boltzmann constant.

Minimization of $\mathcal{F}$ with respect to spin order parameters leads to self-consistent equations

$$\langle S^z_{1,2}\rangle = S\mathcal{B}_S\left(x_{1,2}\right), \tag{14}$$

$$\langle s^z\rangle = s\mathcal{B}_s\left(x_3\right), \tag{15}$$

where the arguments of the Brillouin functions $\mathcal{B}_S\left(\ldots\right)$ and $\mathcal{B}_s\left(\ldots\right)$ are determined respectively by the expressions

$$x_{1,2} = \beta S\left(H^{(m)}_{1,2} + H^{(me)}_{1,2}\right), \tag{16}$$

$$x_3 = \beta S H^{(m)}_3. \tag{17}$$

Equilibrium deformations of all-round compression and uniaxial tension are determined by the relations

$$\langle u_{xx} + u_{yy} + u_{zz}\rangle = \frac{3\left[\alpha(T - T_0) + 24D_1\langle S^z_1\rangle\langle S^z_2\rangle\right]}{V_0\left(c_{11} + 2c_{12}\right)}, \tag{18}$$

$$\langle 2u_{zz} - u_{xx} - u_{yy}\rangle = \frac{24D_2\langle S^z_1\rangle\langle S^z_2\rangle}{V_0\left(c_{11} - c_{12}\right)}. \tag{19}$$

For numerical solution of self-consistent equations, $S = 3/2$ was chosen for magnetic Fe atoms, and $s = 1/2$ for Rh atoms. Elastic coefficients $c_{11} = 218.7$ GPa, $c_{12} = 188.5$ GPa and the volume of the extended elementary cell $V_0 = 216$ Å^3 are taken from work [31].

Unfortunately, the standard use of the molecular-field approach faces a fundamental difficulty. When trying to achieve agreement with experimental data for the temperature dependencies of the total magnetization of FeRh and relative volume change, it turns out that the solution for the ferromagnetic phase with non-zero magnetization of Rh atoms exists throughout the entire temperature range below the Curie point, and moreover, it is energetically more favorable than the antiferromagnetic phase, in which Rh atoms are in a non-magnetic state. It is possible that the appearance of magnetization in the rhodium atoms subsystem is associated with a possible restructuring of spin-polarized states of these atoms, caused by changes in elastic deformations at the AFM–FM transition point [20].

To account for this effect within the phenomenological description, one can transition from the free energy (13), which depends through molecular fields on the magnetizations of iron atoms $\langle S^z_{1,2}\rangle$ and rhodium $\langle s^z\rangle$ to a new thermodynamic potential $\Phi\left(\langle S^z_1\rangle,\langle S^z_2\rangle,\mu\right)$, in which the parameter μ, *internal magnetic field*, acts as an independent variable, whose role is analogous to that of the chemical potential in the grand canonical ensemble. The values μ will be determined by the specified temperature behavior $\langle s^z\rangle$, consistent with the experiment. Formally, the indicated transition to Φ is achieved by a standard substitution (see Appendix)

$$H^{(m)}_3 \to H^{(m)}_3 - \mu \tag{20}$$

in the Hamiltonian (7) and accompanying changes in expressions (13) and (17). In this case, the equation of state (15) should be considered as an implicit equation for determining the field μ.

4. SELECTION OF EXCHANGE PARAMETERS

To perform numerical calculations where the temperature change in the rhodium sublattice magnetization is considered known, we implement a two-pass calculation scheme. In the first stage, we determine the temperature dependence $\langle s^z\rangle$ at $\mu = 0$, using mean-field equations (14), (15) and (18), (19) and achieving good agreement with experimentally observed temperature behaviors of total magnetization and relative volume change $\Delta V/V$ of FeRh compound. It turns out that when choosing exchange parameters close to *ab initio* calculations, the ferromagnetic solution exists throughout the temperature range below the Curie point T_c and always proves to be energetically more favorable compared to the antiferromagnetic solution. Therefore, to set $\langle s^z\rangle$ in the second stage, we will assume that the rhodium magnetization is zero below the AFM-FM transition temperature T_0, determined from experiment, and coincides with the calculated magnetization $\langle s^z\rangle$ of the first pass above T_0.

Let us discuss the choice of model constants. According to *ab initio* calculations [19], the exchange interaction of each iron atom with its first and third neighbor in the Fe subsystem turns out to be negative, which promotes the establishment of AFM order. It turns out that the interaction with the third neighbor weakly depends on the type of reference state (FM or AFM) used in calculations, while the interaction with the first neighbor changes from −8.0 meV for AFM state to values near zero

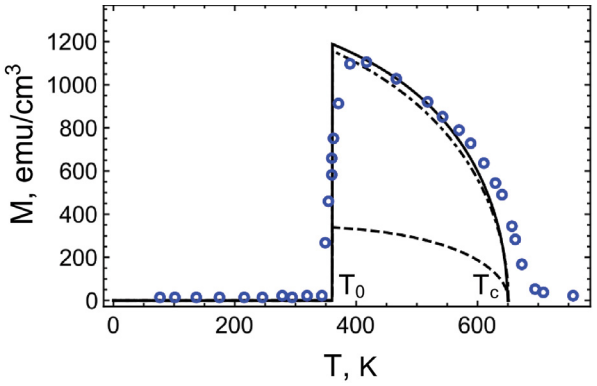

Fig. 2. Temperature dependence of FeRh magnetization (dash-dotted line – first pass, solid line – second pass) and magnetization of Rh atoms in FM phase (dashed line). For comparison, experimental data (open blue circles) taken from work [11]

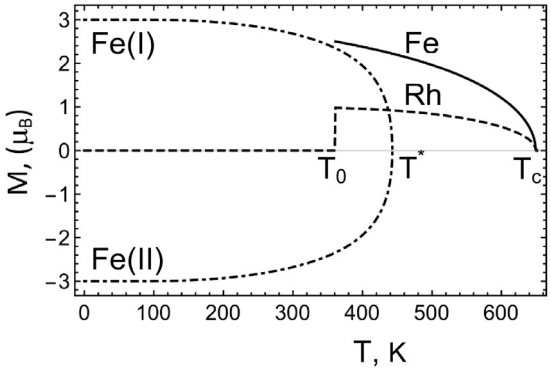

Fig. 3. Temperature dependencies of magnetizations of atoms Fe(I) and Fe(II) in AFM phase and Fe and Rh atoms in FM phase

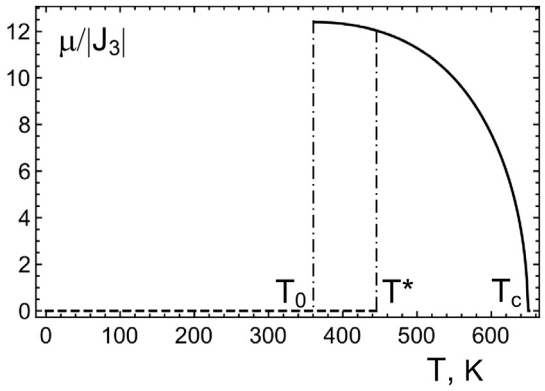

Fig. 4. Temperature dependence of field μ in AFM phase (dashed line) and in FM phase (solid line). The region of first-order AFM–FM transitions is marked with dash-dotted lines

for FM state. In our model, we can associate such a sharp change with the renormalization of exchange interaction between nearest neighbors due to the contribution of magnetoelastic interaction. In this case, the effective exchangeare shown interaction between nearest neighbors is determined by the expression

$$\bar{J}_1 = J_1 + D_1\langle u_{xx} + u_{yy} + u_{zz}\rangle + \\ + \frac{1}{6} D_2\langle 2u_{zz} - u_{xx} - u_{yy}\rangle. \qquad (21)$$

Then the value J_3 can be chosen from the requirement that it coincides with the value $\bar{J}_1$ at $T = 0$, and the relationship between J_2 and J_3 would be close to the value obtained in the *ab initio* ($J_2/J_3 \sim -0.2$) calculation.

For calculating the magnetization of rhodium in the first pass, the following choice of relationships for model exchange and magnetoelastic constants was made:

$$J_1/J_3 = 0.29, \quad J_2/J_3 = -0.18,$$
$$D_1/J_3 = -36.83, \quad D_2/D_1 = 0.1,$$

linking these values with the exchange interaction constant of the iron atom with the third nearest neighbor, for which the value was taken as $J_3 = -3.33 \cdot 10^{-22}$ J. The value of the AFM–FM transition temperature was chosen to be $T_0 = 360$ K. When evaluating the exchange interaction Fe–Rh it should be noted that according to calculations *ab initio*, only the exchange interaction Fe–Fe, is responsible for the stabilization of the AFM state, while the FM order can be stabilized due to sufficiently strong exchange interaction between neighboring iron and rhodium atoms, since in this phase the magnetic moments of Rh are non-zero. In our calculations $J = -6.93J_3$, was taken, which provides a transition temperature to the paramagnetic state of $T_c \approx 650$ K, close to that observed in experiments. The corresponding behavior of the total magnetization FeRh (Fig. 2) shows a jump at T_0 by a value of approximately 1,200 CGS units/cm^3 close to experimentally observed values [11, 32–34]. The same figure shows the temperature dependence of magnetization associated with rhodium atoms.

During the second pass, the constant values were slightly modified

$$J_1/J_3 = 0.31, J/J_3 = -6.6, D_1/J_3 = -31.93,$$

instead of 0.29, -6.93 and -36.83 of the first stage, respectively, the numerical value J_3 was taken

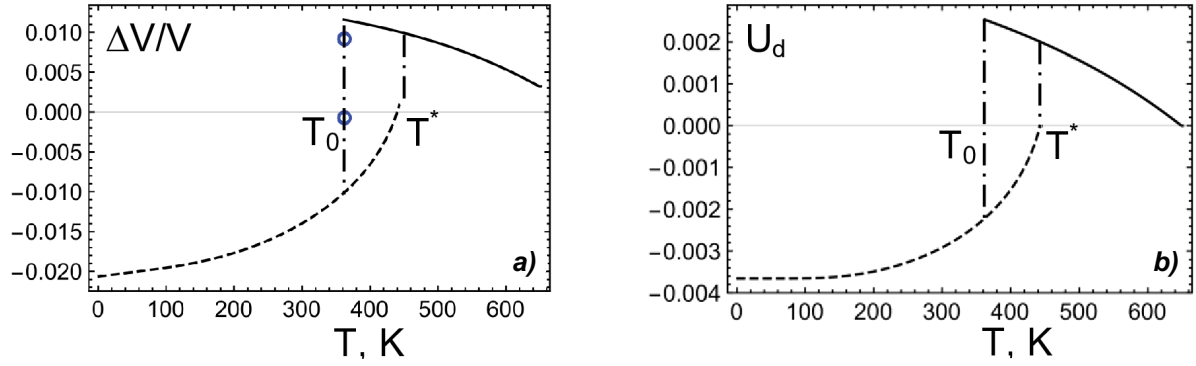

Fig. 5. Temperature dependencies of the relative volume change (a) and uniaxial expansion strain (b). The region of first-order AFM–FM transitions is marked with dash-dotted lines. For comparison, the jump in relative volume change (open blue circles) obtained from experimental data [5] for the lattice constant at temperatures 363 and 364.5 K

as $J_3 = -4.15 \cdot 10^{-22}$ J (instead of $-3.33 \cdot 10^{-22}$ J previously), while other parameters remained unchanged.

The temperature behavior of the magnetizations of iron and rhodium sublattices is shown in Fig. 3. At temperatures below T_0 only the AFM solution is possible. In the temperature range from T_0 to $T^* \approx 440$ K the FM phase emerges, whose free energy is always lower than the free energy of the metastable AFM state, which also exists in this range. This means that the AFM–FM transition is a first-order phase transition, which is consistent with experimental observations [5]. The self-consistent temperature behavior of the field μ is shown in Fig. 4. Based on this calculation, it is reasonable to assume that the jump in the internal field μ in the AFM–FM transition region leads to a relative shift of the partial spin-polarized density of states of the rhodium atom at the Fermi level, which causes the appearance of a non-zero magnetic moment.

The relative volume change, defined by equation (18) and shown in Fig. 5*a*, experiences a jump at the AFM–FM transition point of about 1%, which also agrees well with experimental data [5, 12]. The corresponding behavior of the order parameter associated with uniaxial deformations,

$$U_d = \langle 2u_{zz} - u_{xx} - u_{yy} \rangle / 3,$$

is shown in Fig. 5*b*. The nature and range of change of this value is determined by the sign and magnitude of the constant D_2. The main difference between the temperature behavior of parameters $\Delta V/V$ and U_d appears in the paramagnetic region, where U_d becomes zero, while the relative volume change remains finite due to the thermal expansion effect of the crystal, controlled by the parameter α in expression (6). In our calculations, the value $\alpha = D_1/28$. was chosen. Note that the observation of tetragonal distortions in the region of coexistence of AFM and FM phases was reported in work [35].

Within the framework of the presented model, it is possible to obtain the temperature change of the effective exchange interaction $\tilde{J}_1$, which qualitatively agrees with *ab initio* calculations (Fig. 6). It can be concluded that the specificity of the AFM–FM transition is related to the temperature change of the effective exchange interaction $\bar{J}_1$ of a given iron atom with the nearest neighbors in the first coordination sphere of Fe atoms. The temperature renormalization $\bar{J}_1$ arises due to the contributions of magnetoelastic interaction (21), due to which it is comparable in magnitude and sign with J_3 at $T = 0$ and contributes to the stabilization of the AFM phase. However, as approaches the transition temperature T_0 the value $\bar{J}_1$ sharply decreases and

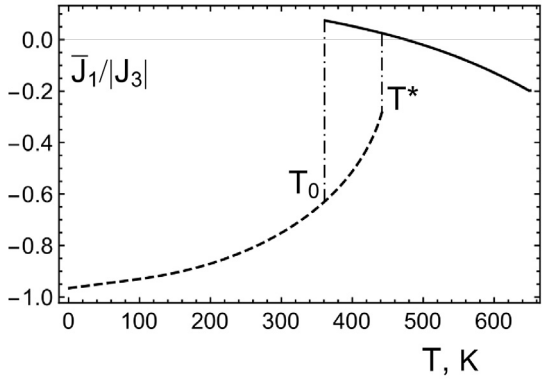

Fig. 6. Temperature change of the effective exchange interaction $\bar{J}_1$ (in units of J_3) of Fe atom a with the first nearest neighbors in the subsystem of iron atoms

takes a small positive value, contributing to the establishment of FM order. The final stabilization of the FM phase occurs due to the spin polarization of Rh atoms, through which the strong ferromagnetic interaction between iron and rhodium atoms, together with $\overline{J}_1$ and J_2 suppresses the competing antiferromagnetic exchange interaction J_3.

5. ACCOUNTING FOR SPIN-WAVE FLUCTUATIONS

Below, using the technique of two-time Green's functions, we analyze changes in equilibrium deformations arising from spin-wave fluctuations. As follows from the magnetoelastic interaction Hamiltonian (4), these corrections are associated with non-zero correlation functions $\langle S^{\alpha}_{\mathbf{m}} S^{\beta}_{\mathbf{n}} \rangle$, in which at least one α or β does not coincide with z. In the Bogoliubov-Tyablikov approximation, where transverse spin fluctuations do not change the z-component of magnetization, only correlation functions of the form

$$\langle S^x_{1\mathbf{m}} S^x_{2\mathbf{n}} \rangle, \quad \langle S^y_{1\mathbf{m}} S^y_{2\mathbf{n}} \rangle, \quad \langle S^x_{1\mathbf{m}} S^y_{2\mathbf{n}} \rangle, \quad \langle S^y_{1\mathbf{m}} S^x_{2\mathbf{n}} \rangle.$$

are non-zero. Let us provide calculation details using the example of the first of these functions, which can be conveniently represented using circular components $S^{\pm} = S^x \pm iS^y$ in the form

$$\langle S^x_{1\mathbf{m}} S^x_{2\mathbf{n}} \rangle = \frac{1}{4}\langle S^-_{1\mathbf{m}} S^+_{2\mathbf{n}} \rangle + \frac{1}{4}\langle S^+_{1\mathbf{m}} S^-_{2\mathbf{n}} \rangle.$$

To calculate the first correlation function on the right side, let us define the retarded Green's functions

$$\langle\langle S^+_{2\mathbf{n}}(t) \mid S^-_{1\mathbf{m}}(0)\rangle\rangle = -i\theta(t)\langle[S^+_{2\mathbf{n}}(t), S^-_{1\mathbf{m}}]\rangle,$$

$$\langle\langle S^+_{1\mathbf{n}}(t) \mid S^-_{1\mathbf{m}}(0)\rangle\rangle = -i\theta(t)\langle[S^+_{1\mathbf{n}}(t), S^-_{1\mathbf{m}}]\rangle,$$

the equations of motion of whose Fourier transforms form a closed system

$$\big[\omega + E_{21}(\mathbf{k})\big]\langle\langle S^+_2 \mid S^-_1\rangle\rangle(\mathbf{k},\omega) -$$

$$-(z_1 J_1(\mathbf{k}) + z_3 J_3(\mathbf{k}))\langle S^z_2\rangle\langle\langle S^+_1 \mid S^-_1\rangle\rangle(\mathbf{k},\omega) = 0, \quad (22)$$

$$\big[\omega + E_{11}(\mathbf{k})\big]\langle\langle S^+_1 \mid S^-_1\rangle\rangle(\mathbf{k},\omega) -$$

$$-(z_1 J_1(\mathbf{k}) + z_3 J_3(\mathbf{k}))\langle S^z_1\rangle\langle\langle S^+_2 \mid S^-_1\rangle\rangle(\mathbf{k},\omega) = 2\langle S^z_1\rangle. \quad (23)$$

Here, the Fourier components of Green's functions are defined

$$\langle\langle S^{\alpha}_{a\mathbf{n}}(t) \mid S^{\beta}_{b\mathbf{m}}(0)\rangle\rangle =$$

$$= \frac{1}{N}\sum_{\mathbf{k}}\int_{-\infty}^{\infty}\frac{d\omega}{2\pi}\exp\big(i\mathbf{k}(\mathbf{n}-\mathbf{m}) - i\omega t\big)\langle\langle S^{\alpha}_a \mid S^{\beta}_b\rangle\rangle(\mathbf{k},\omega),$$

depending on the wave vector $\mathbf{k}$ and frequency ω, and exchange interactions

$$J_1(\mathbf{k}) = \frac{1}{z_1}\sum_{\boldsymbol{\delta}_1} J_1 \cos\big(\mathbf{k}\boldsymbol{\delta}_1\big) =$$

$$= \frac{J_1}{3}\Big[\cos\big(k_x a\big) + \cos\big(k_y a\big) + \cos\big(k_z a\big)\Big],$$

$$J_2(\mathbf{k}) = \frac{1}{z_2}\sum_{\boldsymbol{\delta}_2} J_2 \cos\big(\mathbf{k}\boldsymbol{\delta}_2\big) =$$

$$= \frac{J_2}{3}[\cos\big(k_x a\big)\cos\big(k_y a\big) + \cos\big(k_x a\big)\cos\big(k_z a\big) +$$

$$+\cos\big(k_y a\big)\cos\big(k_z a\big)],$$

$$J_3(\mathbf{k}) = \frac{1}{z_3}\sum_{\boldsymbol{\delta}_3} J_3 \cos\big(\mathbf{k}\boldsymbol{\delta}_3\big) = \cos\big(k_x a\big)\cos\big(k_y a\big)\cos\big(k_z a\big),$$

and abbreviated notations are introduced

$$E_{11}(\mathbf{k}) = z_1 J_1\langle S^z_2\rangle + z_2\big[J_2 - J_2(\mathbf{k})\big]\langle S^z_1\rangle +$$

$$+z_3 J_3\langle S^z_2\rangle + \frac{1}{2}z_4 J\langle s^z\rangle, \quad (24)$$

$$E_{21}(\mathbf{k}) = z_1 J_1\langle S^z_1\rangle + z_2\big[J_2 - J_2(\mathbf{k})\big]\langle S^z_2\rangle +$$

$$+z_3 J_3\langle S^z_1\rangle + \frac{1}{2}z_4 J\langle s^z\rangle. \quad (25)$$

From the system (22), (23) we find

$$\langle\langle S^+_2 \mid S^-_1\rangle\rangle(\mathbf{k},\omega) = \frac{2B(\mathbf{k})\langle S^z_1\rangle\langle S^z_2\rangle}{\big[\omega - \omega_1(\mathbf{k})\big]\big[\omega - \omega_2(\mathbf{k})\big]},$$

where

$$B(\mathbf{k}) = z_1 J_1(\mathbf{k}) + z_3 J_3(\mathbf{k}),$$

and eigenfrequencies are determined by expressions

$$\omega_{1,2}(\mathbf{k}) = -\frac{E_{11}(\mathbf{k}) + E_{21}(\mathbf{k})}{2} \pm$$

$$\pm\frac{1}{2}\sqrt{(E_{11}(\mathbf{k}) - E_{21}(\mathbf{k}))^2 + 4B^2(\mathbf{k})\langle S^z_1\rangle\langle S^z_2\rangle}. \quad (26)$$

We use the relation between the Green's function discontinuity when crossing the real axis with the spectral density

$$\mathcal{J}_{S_2^+S_1^-}(\mathbf{k},\omega) = -in_B(\omega)[\langle\langle S_2^+ \mid S_1^-\rangle\rangle(\mathbf{k},\omega - i\varepsilon) - \\ -\langle\langle S_2^+ \mid S_1^-\rangle\rangle(\mathbf{k},\omega + i\varepsilon)], \quad (27)$$

which gives

$$\mathcal{J}_{S_2^+S_1^-}(\mathbf{k},\omega) = \frac{4\pi n_B(\omega)B(\mathbf{k})\langle S_1^z\rangle\langle S_2^z\rangle}{\omega_1(\mathbf{k}) - \omega_2(\mathbf{k})} \times \\ \times\big[\delta\big(\omega - \omega_1(\mathbf{k})\big) - \delta\big(\omega - \omega_2(\mathbf{k})\big)\big]. \quad (28)$$

Here

$$n_B(\omega) = \big[\exp(\beta\omega) - 1\big]^{-1}$$

is the Bose distribution function.

Then the sought correlation function

$$\langle S_{1\mathbf{m}}^- S_{2\mathbf{n}}^+\rangle = \frac{1}{N}\sum_{\mathbf{k}}\int_{-\infty}^{\infty}\frac{d\omega}{2\pi}\mathcal{J}_{S_2^+S_1^-}(\mathbf{k},\omega)e^{i\mathbf{k}(\mathbf{m}-\mathbf{n})} = \\ = \frac{2\langle S_1^z\rangle\langle S_2^z\rangle}{N}\times \\ \times\sum_{\mathbf{k}}B(\mathbf{k})\frac{n_B\big(\omega_1(\mathbf{k})\big) - n_B\big(\omega_2(\mathbf{k})\big)}{\omega_1(\mathbf{k}) - \omega_2(\mathbf{k})}e^{i\mathbf{k}(\mathbf{m}-\mathbf{n})}. \quad (29)$$

Similar calculation leads to the expression

$$\langle S_{1\mathbf{m}}^+ S_{2\mathbf{n}}^-\rangle = \frac{2\langle S_1^z\rangle\langle S_2^z\rangle}{N}\times \\ \times\sum_{\mathbf{k}}B(\mathbf{k})\frac{n_B\big(\tilde{\omega}_1(\mathbf{k})\big) - n_B\big(\tilde{\omega}_2(\mathbf{k})\big)}{\tilde{\omega}_1(\mathbf{k}) - \tilde{\omega}_2(\mathbf{k})}e^{i\mathbf{k}(\mathbf{m}-\mathbf{n})}, \quad (30)$$

in which

$$\tilde{\omega}_{1,2}(\mathbf{k}) = \frac{E_{11}(\mathbf{k}) + E_{21}(\mathbf{k})}{2} \pm \\ \pm\frac{1}{2}\sqrt{(E_{11}(\mathbf{k}) - E_{21}(\mathbf{k}))^2 + 4B^2(\mathbf{k})\langle S_1^z\rangle\langle S_2^z\rangle}. \quad (31)$$

Then we have

$$\langle S_{1\mathbf{m}}^x S_{2\mathbf{n}}^x\rangle = -\frac{\langle S_1^z\rangle\langle S_2^z\rangle}{2N}\times \\ \times\sum_{\mathbf{k}}B(\mathbf{k})\frac{\left[\frac{\beta}{2}\big(\tilde{\omega}_1(\mathbf{k}) - \tilde{\omega}_2(\mathbf{k})\big)\right]}{\left[\frac{\beta}{2}\tilde{\omega}_1(\mathbf{k})\right]\left[\frac{\beta}{2}\tilde{\omega}_2(\mathbf{k})\right]\big(\tilde{\omega}_1(\mathbf{k}) - \tilde{\omega}_2(\mathbf{k})\big)}\times \\ \times e^{i\mathbf{k}(\mathbf{m}-\mathbf{n})}. \quad (32)$$

Obviously,

$$\langle S_{1\mathbf{m}}^y S_{2\mathbf{n}}^y\rangle = \langle S_{1\mathbf{m}}^x S_{2\mathbf{n}}^x\rangle. \quad (33)$$

It can be shown, without resorting to explicit calculations, that

$$\langle S_{1\mathbf{m}}^x S_{2\mathbf{n}}^y\rangle = -\langle S_{1\mathbf{m}}^y S_{2\mathbf{n}}^x\rangle, \quad (34)$$

and since (4) includes their sum, these correlation functions do not contribute additionally to the magnetoelastic interaction.

Spin-wave excitations make an additional contribution to the free energy of the extended unit cell, associated with magnetoelastic interactions

$$\tilde{\mathcal{F}}_{me} = 48D_1\big(\tilde{u}_{xx} + \tilde{u}_{yy} + \tilde{u}_{zz}\big)\gamma(T)\langle S_1^z\rangle\langle S_2^z\rangle - \\ -4D_2\big(2\tilde{u}_{zz} - \tilde{u}_{xx} - \tilde{u}_{yy}\big)\gamma(T)\langle S_1^z\rangle\langle S_2^z\rangle,$$

in which the result (32) for nearest neighbors is presented in the form

$$\langle S_1^x S_2^x\rangle = \langle S_1^y S_2^y\rangle = -\gamma(T)\langle S_1^z\rangle\langle S_2^z\rangle$$

and the tensor of elastic deformations is defined $\tilde{u}_{ij}$, caused by spin-wave excitations.

This change in free energy is compensated by a corresponding contribution associated with elastic interactions

$$\tilde{\mathcal{F}}_e = \frac{1}{2}c_{11}V_0(\tilde{u}_{xx}^2 + \tilde{u}_{yy}^2 + \tilde{u}_{zz}^2) + \\ + c_{12}V_0(\tilde{u}_{xx}\tilde{u}_{yy} + \tilde{u}_{xx}\tilde{u}_{zz} + \tilde{u}_{yy}\tilde{u}_{zz}) + \\ + 2c_{44}V_0(\tilde{u}_{yz}^2 + \tilde{u}_{xz}^2 + \tilde{u}_{xy}^2),$$

which determines the corresponding additions to the equilibrium deformations of uniform compression

$$\langle\tilde{u}_{xx} + \tilde{u}_{yy} + \tilde{u}_{zz}\rangle = -\gamma(T)\frac{144D_1\langle S_1^z\rangle\langle S_2^z\rangle}{V_0\big(c_{11} + 2c_{12}\big)}, \quad (35)$$

and uniaxial tension

$$\langle 2\tilde{u}_{zz} - \tilde{u}_{xx} - \tilde{u}_{yy}\rangle = \gamma(T)\frac{24D_2\langle S_1^z\rangle\langle S_2^z\rangle}{V_0\big(c_{11} - c_{12}\big)}. \quad (36)$$

Taking into account the cubic symmetry of the crystal, the temperature-dependent coefficient γ can be represented as

$$\gamma(T) = \frac{1}{2N}\sum_{\mathbf{k}}S(\mathbf{k})B(\mathbf{k})\times \\ \times\frac{\mathrm{sh}\left[\frac{\beta}{2}\big(\tilde{\omega}_1(\mathbf{k}) - \tilde{\omega}_2(\mathbf{k})\big)\right]}{\mathrm{sh}\left[\frac{\beta}{2}\tilde{\omega}_1(\mathbf{k})\right]\mathrm{sh}\left[\frac{\beta}{2}\tilde{\omega}_2(\mathbf{k})\right]\big(\tilde{\omega}_1(\mathbf{k}) - \tilde{\omega}_2(\mathbf{k})\big)}, \quad (37)$$

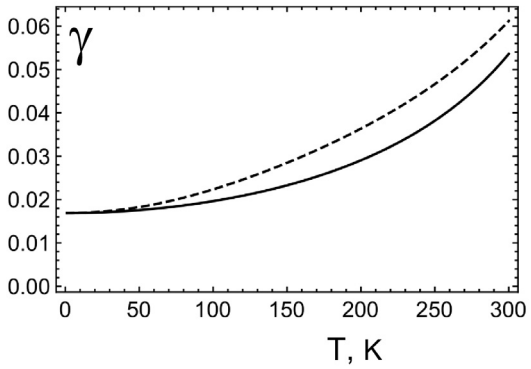

Fig. 7. Temperature change of γ: dashed curve numerical calculation according to formula (37), solid curve analytical approximation $\gamma_0 + \gamma_1$, determined by equations (41) and (43)

where the structural form factor is defined

$$S(\mathbf{k}) = \frac{1}{3}\left[\cos\left(k_x a\right) + \cos\left(k_y a\right) + \cos\left(k_z a\right)\right].$$

Combining expressions (35), (36) with the corresponding results for the mean field (18), (19), we obtain the final result:

$$\langle u_{xx} + u_{yy} + u_{zz}\rangle = \frac{3\left[\alpha(T - T_0) + 24\tilde{D}_1\langle S_1^z\rangle\langle S_2^z\rangle\right]}{V_0\left(c_{11} + 2c_{12}\right)}, \quad (38)$$

$$\langle 2u_{zz} - u_{xx} - u_{yy}\rangle = \frac{24\tilde{D}_2\langle S_1^z\rangle\langle S_2^z\rangle}{V_0\left(c_{11} - c_{12}\right)}, \quad (39)$$

in which the role of spin-wave fluctuations is reduced to temperature renormalization of magnetoelastic coupling constants

$$\tilde{D}_1 = D_1\left[1 - 2\gamma(T)\right],$$

$$\tilde{D}_2 = D_2\left[1 + \gamma(T)\right].$$

To estimate γ in the low-temperature region, $T \ll T_0$, it is convenient to represent expression (37) as

$$\gamma(T) = -\frac{1}{N}\sum_{\mathbf{k}}\frac{S(\mathbf{k})B(\mathbf{k})}{\omega_1(\mathbf{k})}\left[n_B\left(\omega_1(\mathbf{k})\right) + \frac{1}{2}\right], \quad (40)$$

in which one can distinguish the part associated with zero-point oscillations and weakly dependent on temperature:

$$\gamma_0 = -\frac{1}{2N}\sum_{k}\frac{S(k)B(k)}{\omega_1(k)} \quad (41)$$

and the contribution associated with thermal excitation of magnons:

$$\gamma_1(T) = -\frac{1}{N}\sum_{\mathbf{k}}\frac{S(\mathbf{k})B(\mathbf{k})}{\omega_1(\mathbf{k})}n_B\left(\omega_1(\mathbf{k})\right). \quad (42)$$

The analytical estimate (42) leads to the expression

$$\gamma_1(T) \approx \frac{\sqrt{3}}{4}\frac{(k_B T)^2}{\left|\langle S_2^z\rangle\right|^3}\left|z_1 J_1 - 2z_2 J_2 + 3z_3 J_3\right|^{-\frac{3}{2}} \times \left|z_1 J_1 + z_3 J_3\right|^{-\frac{1}{2}}. \quad (43)$$

The graph of temperature behavior $\gamma(T)$ is shown in Fig. 5. Obviously, the magnitude of temperature renormalization of magnetoelastic coupling constants is several percent. Due to the positivity of γ temperature increase reduces $\tilde{D}_1$, which leads to a decrease in uniform compression deformation due to spin fluctuations and, conversely, thermal excitation of spin waves contributes to an increase in $\tilde{D}_2$, controlling the magnitude of uniaxial tension deformation.

6. CONCLUSIONS

In this work, an effective mean-field theory is proposed to explain the features of magnetic phase transitions in FeRh alloy, which takes into account elastic degrees of freedom and their interaction with the magnetic subsystem. Considering the key role of rhodium in the magnetic behavior of this alloy, a distinctive feature of our description is that instead of the average magnetization of rhodium atoms, the traditional order parameter in the statistical model of the canonical ensemble, we consider the "internal" magnetic field conjugate to Rh magnetization as the order parameter, whose temperature evolution is determined selfconsistently along with the magnetizations of iron atoms in the first and second sublattices and the order parameters of the elastic subsystem, describing the deformation of uniform compression and uniaxial tension. If we assume that the temperature behavior of rhodium magnetization is known, then such consideration corresponds to the statistical model of the grand canonical ensemble. The introduction of the internal magnetic field allows effectively taking into account the splitting of spin-polarized densities of Rh electronic

states at the Fermi level, which is responsible for the emergence of a non-zero magnetic moment.

Within the framework of the presented approach, it is possible to calculate the temperature dependencies of total magnetization and relative volume change, which are in good agreement with experimental data across the entire temperature range, and to show that the AFM–FM transition represents a first-order phase transition. The emergence of elastic fluctuations that lower the lattice symmetry to tetragonal is explained, and their enhancement due to thermal excitation of spin waves is demonstrated. The selection of exchange interaction constants, consistent with *ab initio* calculations of electronic structure, allowed identifying the leading mechanism of the AFM–FM transition – the renormalization of exchange interaction between magnetic moments of nearest neighbors in the iron atoms subsystem by two-ion magnetoelastic interaction.

A sharp increase in the internal magnetic field in the region of the AFM–FM transition, causing the appearance of a magnetic moment in Rh atoms and accompanied by a sharp change in lattice deformations, suggests that it is the elastic deformations caused by *changes in lattice parameters* during doping of FeRh with magnetic ions that are responsible for significant changes in the AFM–FM transition temperature (both increasing and decreasing) [23], rather than the *stabilization of the FM phase* by magnetic moments of the doped ions. Lattice distortions can notably affect the relative shift of partial densities of spin-polarized electronic states of Rh at the Fermi level. To verify this assumption, further targeted experimental studies and corresponding *ab initio* calculations are needed.

FUNDING

This work was supported by the Ministry of Science and Higher Education of the Russian Federation, state assignment project FEUZ-2023-0017 (A.S.O.), theme "Potok" No. 122021000031-8 (E.Z.V.) and "Magnit" No.122021000034-9 (N.V.B.). The work of I.S.K. was supported by the Ministry of Science and Higher Education of the Russian Federation (Ural Federal University Development Program within the Priority-2030 Program). The work of A.A.T. was carried out with financial support from the "BASIS" Foundation for the Development of Theoretical Physics and Mathematics.

APPENDIX.
FIELD μ AND THE PRINCIPLE OF MAXIMUM INFORMATION ENTROPY

Suppose that the system can be in one of N states and the probability of finding it in the kth state equals $p_k (k = 1,\ldots,N)$. Let the system energy E and magnetization of rhodium atoms s^z (per unit cell) take values E_k and s_k^z, when the system is in state k. Consider a situation where the average values E and $\langle s^z \rangle$ for the system are fixed, and determine using the method of Lagrange multipliers [36] the distribution function p_k, corresponding to the maximum of information entropy

$$S = -k_B \sum_k p_k \ln p_k$$

with additional conditions

$$E = \sum_k p_k E_k, \quad \langle s^z \rangle = \sum_k p_k s_k^z.$$

Determining the extremum of expression

$$f = -k_B \sum_k \left(p_k \ln p_k - \alpha p_k + \beta E_k + \beta \mu s_k^z \right), \quad (44)$$

in which additional conditions are taken into account using undetermined multipliers α, β and μ, we obtain the desired distribution

$$p_k = \frac{1}{\Xi} \exp\left(-\beta E_k - \beta \mu s_k^z \right), \quad (45)$$

where

$$\Xi = \sum_k \exp\left(-\beta E_k - \beta \mu s_k^z \right).$$

While

$$\langle s^z \rangle = -\frac{1}{\beta} \frac{\partial}{\partial \mu} \ln \Xi. \quad (46)$$

From expression (45) it follows that if the energy of the magnetic subsystem is determined by expression (7), then the obtained distribution reduces to the standard canonical distribution with renormalization of the molecular field acting on the spin of rhodium atom (20). Taking into account the explicit expression for

$$H_3^{(m)} = z_4 J \left(\langle S_1^z \rangle + \langle S_2^z \rangle \right), \quad J > 0,$$

we can conclude that in the AFM phase, when $H_3^{(m)} = 0$, the appearance of field $\mu > 0$ is unfavorable, as this would lead to a decrease in probability (45). In the FM phase μ will be directed antiparallel to $H_3^{(m)}$.

REFERENCES

1. M. Fallot, Ann. Phys.(Paris) **10**, 291 (1938).
2. M. Fallot and R. Horcart, Rev. Sci. **77**, 498 (1939).
3. J. B. Staunton, R. Banerjee, M. dos S. Dias et al., Phys. Rev. B **89**, 054427 (2014).
4. L. Muldawer and F. de Bergevin, J. Chem. Phys. 35, 1257 (1961).
5. A. I. Zakharov, A. M. Kadomtseva, R. Z. Levitin et al., JETP **46**, 2003 (1964).
6. N. A. Zarkevich and D. D. Jonson, Phys. Rev. B **97**, 014202 (2018).
7. G. Shirane, C. W. Chen, P. A. Flin et al., J. Appl. Phys. Suppl. **33**, 1044 (1963).
8. G. Shirane, R. Nathans, and C. W. Chen, Phys. Rev. **134**, A1547 (1964).
9. J. S. Couvel, J. Appl. Phys. **37**, 1257 (1966).
10. M. P. Annaorazov, K. A. Asatryan, G. Myalikgulyev et al., Cryogenics **32**, 867 (1992).
11. J. S. Kouvel and J. Hartelius, J. Appl. Phys. **33**, 1343 (1962).
12. M. R. Ibarra and Algarabel, Phys. Rev. B **50**, 4196 (1994).
13. R. R. Gimaev, A. A. Vaulin, A. F. Gubkin et al., FMM **121**, 907 (2020).
14. C. Kittel, Phys. Rev. **120**, 335 (1960).
15. C. P. Bean and D. S. Rotbell, Phys. Rev. **126**, 104 (1962).
16. E. Valiev, R. Gimaev, V. Zverev et al., Intermetallics **108**, 81 (2019).
17. M. E. Gruner, T. Hoffman, and P. Entel, Phys. Rev. B **67**, 064415 (2003).
18. L. M. Sandratckii and P. Navropoulos, Phys. Rev. B **83**, 174408 (2011).
19. S. Polesya, S. Mankovsky, D. Ködderitzsch et al., Phys. Rev. B **93**, 024423 (2016).
20. M. I. Kurkin, A. V. Telegin, P. A. Agzamova et al., FMM **123**, 579 (2022).
21. G. Ju, J. Hohlfeld, B. Bergman et al., Phys. Rev. Lett. **93**, 197403 (2004).
22. S. O. Mariager, F. Pressacco, G. Ingold et al., Phys. Rev. Lett. **108**, 087201 (2012).
23. S. Yuasa, Y. Otani, H. Miyajima et al., IEEE Trans. J. Mag. Jpn. **9** (6), 202 (1994).
24. K. Nishihara, Y. Nakazawa, L. Li et al., Mater. Trans. **49**, 753 (2008).
25. A. S. Komlev, G. F. Cabeza, A.M. Chirkova et al. Metals **13**, 1650 (2023).
26. A. S. Komlev, R. A. Makarin, K. P. Skokov et al., Metall. Mater. Trans. A **54**, 3683 (2023).
27. G. A. Smolensky (ed.), V. V. Lemanov, G. M. Nedlin et al., *Physics of Magnetic Dielectrics*, Nauka, Leningrad (1974).
28. E. Callen, Phys. Rev. 139, A455 (1965).
29. L. D. Landau, E. M. Lifshitz, *Theory of Elasticity, Nauka*, Moscow (1965).
30. S. V. Vonsovsky, M. I. Katsnelson, *Quantum Physics of Solids*, Nauka, Moscow (1983).
31. W. He, H. Huang, and X. Ma, Materials Lett. **195**, 156 (2017).
32. S. Maat, J.-U. Thiele, and E. E. Fullerton, Phys. Rev. B **72**, 214432 (2005).
33. J. Cao, N.T. Nam, S. Inoue et al., J. Appl. Phys. **103**, 07F501 (2008).
34. I. Suzuki, T. Koike, M. Itoh et al., J. Appl. Phys. **105**, 07E501 (2009).
35. A. I. Zakharov, FMM **24**, 84 (1967).
36. *Problems in Thermodynamics and Statistical Physics*, ed. P. Landsberg, Mir, Moscow (1974).